

EXPERIMENTAL MEASUREMENTS OF INGESTION THROUGH TURBINE RIM SEALS.

PART 2: ROTATIONALLY-INDUCED INGRESS

Carl M Sangan
 Oliver J Pountney

Kunyuan Zhou*
 Mike Wilson

J Michael Owen
 Gary D Lock

Dept. of Mechanical Engineering
 University of Bath
 Bath, BA2 7AY
 United Kingdom

* Dept. of Engineering Thermophysics
 School of Jet Propulsion
 Beihang University
 Beijing, 100191 P.R.China

ABSTRACT

Part 1 of this two-part paper presented experimental results for externally-induced (EI) ingress, where the ingestion of hot gas through the rim seal into the wheel-space of a gas turbine is controlled by the circumferential variation of pressure in the external annulus. In Part 2, experimental results are presented for rotationally-induced (RI) ingress, where the ingestion is controlled by the pressure generated by the rotating fluid in the wheel-space. Although EI ingress is the common form of ingestion through turbine rim seals, RI ingress or combined ingress (where EI and RI ingress are both significant) is particularly important for double seals, where the pressure asymmetries are attenuated in the annular space between the inner and outer seals.

In this paper, the sealing effectiveness was determined from concentration measurements, and the variation of effectiveness with sealing flow rate was compared with theoretical curves for RI ingress obtained from an orifice model. Using a nondimensional sealing parameter, Φ_0 , the data could be collapsed onto a single curve, and the theoretical variation of effectiveness with Φ_0 was in very good agreement with the data for a wide range of flow rates and rotational speeds. It was shown that the sealing flow required to prevent RI ingress was much less than that needed for EI ingress, and it was also shown that the effectiveness of a radial-clearance seal is significantly better than that for an axial-clearance seal for both EI and RI ingress.

NOMENCLATURE

b radius of seal
 c concentration
 $C_{d,e}$ $C_{d,i}$ discharge coefficients for egress, ingress
 C_p pressure coefficient $[= (p_2 - \bar{p}_2) / (l/2 \rho \Omega^2 b^2)]$

C_w nondimensional flow rate $[= \dot{m} / \mu b]$
 $C_{w,e}, C_{w,i}$ values of C_w for egress, ingress
 $C_{w,o}$ nondimensional sealing flow rate
 $C_{w,min}$ minimum value of $C_{w,o}$ to prevent ingress
 $C_{\beta 1}$ modified internal swirl ratio $[= \beta_1^2 / (1 - r_1^2 / r_2^2)]$
 $C_{\beta 2}$ modified external swirl ratio $[= \beta_2^2 / (r_2^2 / r_1^2 - 1)]$
 G_c seal-clearance ratio $[= s_c / b]$
 \dot{m} mass flow rate
 p absolute static pressure
 \bar{p} mean absolute static pressure over one vane pitch
 r radius
 Re_ϕ rotational Reynolds number $[= \rho \Omega b^2 / \mu]$
 s axial clearance between rotor and stator
 s_c seal clearance
 U bulk mean velocity of sealing flow $[= \dot{m} / 2\pi r b s_c]$
 V_ϕ tangential component of velocity
 ΔC_p nondimensional pressure difference
 $[= \Delta p / (l/2 \rho \Omega^2 b^2)]$
 Δp peak-to-trough pressure difference in annulus
 $[= p_{2,max} - p_{2,min}]$
 β swirl ratio $[= V_\phi / \Omega r]$
 Γ_c ratio of discharge coefficients $[= C_{d,i} / C_{d,e}]$
 Γ_p pressure parameter $[= C_p / C_{\beta 1}]$
 Γ_T summation of Γ parameters
 Γ_β swirl parameter $[= C_{\beta 1} / C_{\beta 2} \approx (\beta_2 / \beta_1)^2]$
 $\Gamma_{\Delta p}$ external pressure parameter $[= \Delta C_p / C_{\beta 1}]$
 δ radial growth
 ε sealing effectiveness $[= C_{w,o} / C_{w,e} = \Phi_0 / \Phi_e]$
 ε_c concentration effectiveness $[= (c_s - c_a) / (c_o - c_a)]$
 Φ nondimensional sealing parameter $[= C_w / (2\pi G_c Re_\phi)]$
 Φ_i value of Φ when $C_w = C_{w,i}$
 Φ_i^* value of Φ_i when $\Phi_0 = 0$

Φ_{min}	value of Φ when $C_w = C_{w,min}$
Φ_0	value of Φ when $C_w = C_{w,0}$
ϕ	angular coordinate, non-dimensional vane pitch
λ_T	turbulent flow parameter [$= C_w Re_\phi^{-0.8}$]
μ	dynamic viscosity
ρ	density
Ω	angular velocity of rotating disc

Subscripts

a	annulus
CI	combined ingress
e	egress
EI	externally-induced ingress
i	ingress
max	maximum
min	minimum
o	superposed flow, zero rotation
RI	rotationally-induced ingress
$1,2$	locations in wheel-space and annulus
*	value when $C_{w,o}=0$

1. INTRODUCTION

Fig. 1 illustrates a typical high-pressure gas-turbine stage where cooling air limits the metal temperatures to ensure the integrity and operating life of the blades, vanes and discs. The discs are cooled by a radially-outward flow of air extracted from the compressor, which removes heat conducted from the blades. The cooling air also performs a sealing function, reducing the ingress of hot mainstream gas into the wheel-space (or cavity) between the rotating disc and the adjacent stationary casing. The sealing flow is expelled from the wheel-space into the main gas-path annulus through the clearance separating the rotating and stationary surfaces.

The diversion of compressed air and its subsequent mixing with the main-gas flow exact penalties on the performance of the machine, and so seals are fitted near the periphery of the disc to accomplish the tasks of sealing the cavity and cooling the metal with a minimum of mass flow. An example of a typical rim seal, located at the base of a rotor blade near the position of disc-attachment, is shown in the inset in Fig. 1.

As explained in Part 1 [1] of this two-part paper, hot-gas ingestion through turbine rim seals is caused principally by the circumferential variation of pressure in the external annulus. The three-dimensional pressure variation is created by the axial mainstream flow passing over the stationary nozzle guide vanes and the rotating turbine blades. Ingress of hot gas through the seal clearance occurs where the external pressure is higher than that in the wheel-space, and the egress of sealing air, mixed with the ingested gas, occurs where the external pressure is lower. This type of ingestion is referred to as *externally-induced (EI) ingress*.

There is, however, another cause of ingress, which can occur even when the external flow is axisymmetric. The rotating fluid in the wheel-space creates a centripetal acceleration and a

consequential radial gradient of pressure. The resulting pressure in the wheel-space increases with increasing radius, which means that the internal pressure can be smaller than that in the fluid outside the wheel-space. This pressure difference creates ingress of external fluid through the seal clearance, and the ‘disc-pumping effect’ creates egress near the rotating turbine disc. This type of ingestion is referred to as *rotationally-induced (RI) ingress*, which is the subject of this paper.

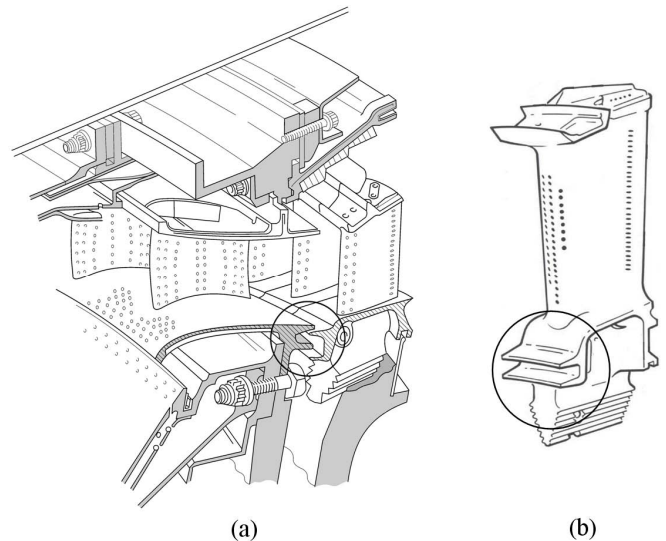


Fig 1: (a) Cooled turbine stage; (b) Double seal on blade

In many practical cases, RI ingress is negligible. However, there are some cases where its magnitude is similar to that of EI ingress; these cases are referred to as *combined ingress*. As stated by Owen *et al.* [2], it is quite probable that some previously published ingress experiments which were thought to have been conducted in the EI regime may well have been in the combined-ingress regime. More importantly, combined ingress can occur in double seals, like those illustrated in Fig. 1. Here the pressure asymmetries created in the external annulus are attenuated in the annular space between the inner and outer seals: EI ingress occurs through the outer seal and combined (or in the limit RI) ingress occurs through the inner seal. RI ingress is therefore not of academic interest alone, it is also of practical importance for the seal designer.

The aim of the theoretical, computational and experimental research at the University of Bath is to provide a fundamental understanding of the ‘ingress problem’ and to produce data and procedures that will lead to improved designs of rim seals. Although the fluid mechanics is complex, the authors have developed simple orifice models for EI, RI and combined ingress [2-5], and the resulting orifice equations have been solved analytically to provide *implicit* relationships between the sealing effectiveness and the sealing flow rate.

In this paper, *explicit* solutions of the orifice equations for RI and EI ingress are given in Appendices A and B, and a review of RI ingress and the orifice model is given in Section 2

below. Experimental results for two different rim seals, and comparison between the measured and theoretical sealing effectiveness, are presented in Section 3. Some practical implications are discussed in Section 4, and the principal conclusions of this research are summarised in Section 5.

2. REVIEW OF PREVIOUS WORK

As ingress has been extensively reviewed by Owen *et al.* [2-5], only a brief review of the papers that are relevant to RI ingress is included here. Symbols are defined in the Nomenclature.

2.1 RI ingress

One of the earliest studies into the phenomenon of ingestion was undertaken at the University of Sussex by Bayley and Owen [6] who investigated experimentally a shrouded stator separated axially from a rotor. The Sussex rig, which incorporated an axial-clearance rim seal, operated without an external annulus and without external flow. A superposed radial flow of air discharged through the seal clearance, s_c , at radius b into the quiescent atmosphere. Owing to the sub-atmospheric pressure created by the rotating fluid in the system, external (atmospheric) air could be drawn into the wheel-space. Increasing the superposed radial flow rate increased the relative pressure inside the wheel-space and consequently reduced the amount of ingested air; at sufficiently high superposed flow rates, ingress did not occur.

Bayley and Owen identified the following important non-dimensional parameters: $C_{w,o}$, the non-dimensional sealing flow rate; G_c the seal-clearance ratio; and Re_ϕ , the rotational Reynolds number. The definitions are:

$$G_c = \frac{s_c}{b}, Re_\phi = \frac{\rho \Omega b^2}{\mu}, C_{w,o} = \frac{\dot{m}_o}{\mu b} \quad (2.1)$$

where undefined symbols can be found in the Nomenclature. Using a simple fluid-dynamic model, in which the seal clearance was treated as an orifice, they showed that $C_{w,min}$, the nondimensional sealing flow rate required to prevent ingestion, was proportional to Re_ϕ and to G_c , proposing what is now termed the *Bayley-Owen criterion* for RI ingress:

$$C_{w,min} = 0.61 G_c Re_\phi \quad (2.2)$$

This criterion, which was based on pressure measurements for $G_c = 0.0033$ and 0.0067 and $Re_\phi < 4 \times 10^6$, applies only to axial-clearance seals.

Much of the subsequent published research into RI ingress was conducted at Sussex [7-13] and at Hartford in the United States [14, 15]. In particular, Graber *et al.* [15] reported extensive concentration measurements in a rotating-disc rig, which was used to determine the effects of seal geometry, rotational Reynolds numbers and the level of swirl in the external annulus on the sealing effectiveness. The axial velocity in the annulus was very small (< 0.03 m/s), and as the authors did not report a circumferential variation in pressure, it is likely

that the flow in the annulus was very close to axisymmetric and consequently RI ingress occurred. Their results showed that the external swirl made no significant difference to the effectiveness.

2.2 Orifice model for RI ingress

Orifice models recently developed at the University of Bath [2-5] have had good success in calculating the sealing effectiveness of rim seals for both RI and EI ingress. The orifice equations are based on two standard fluid dynamic models: (i) the orifice model for flow from a large reservoir through a small nozzle; (ii) the actuator disc where there is discontinuous pressure change across an imaginary surface.

The mathematical model is based on a *sealing ring*, as shown in Fig. 2. Ingress and egress simultaneously cross different parts of an imaginary surface, which can be thought of as a thin, permeable membrane with the same dimensions as the seal clearance. Egress starts in the wheel-space where the static pressure is p_1 and, after crossing the sealing ring, emerges in the external annulus, where the static pressure is p_2 ; conversely, ingress starts in the annulus and emerges in the wheel-space.

The model uses variations of Bernoulli's equation, including swirl terms, to relate the sealing flow rate to the pressure drop across the seal. Although the equations are derived for inviscid incompressible flow, discharge coefficients, analogous to those used for the standard orifice equations, are introduced to account for losses. In general, different discharge coefficients ($C_{d,i}$ and $C_{d,e}$) are needed for ingress and egress, and these have to be determined empirically for each seal geometry.

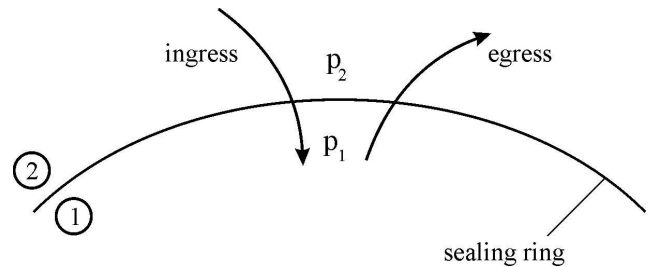


Fig. 2: Sealing-ring model

Only the principal solutions of the orifice model are given below, and for details of their derivation the reader is referred to the papers cited in the text; the *explicit* effectiveness equations are derived in the Appendix of this paper.

Owen [3] showed that the radial components of egress and ingress can then be expressed as

$$\frac{V_{r,e}}{\Omega b} = C_{d,e} \sqrt{C_{\beta_1} - C_p} \quad (2.3)$$

when $C_{\beta_1} \geq C_p$, and

$$\frac{V_{r,i}}{\Omega b} = C_{d,i} \sqrt{C_p - C_{\beta_2}} \quad (2.4)$$

when $C_p \geq C_{\beta_2}$, where

$$C_p = \frac{p_2 - p_1}{1/2 \rho \Omega^2 b^2}, C_{\beta_1} = \beta_1^2 \left(1 - \frac{r_1^2}{r_2^2}\right), C_{\beta_2} = \beta_2^2 \left(\frac{r_2^2}{r_1^2} - 1\right) \quad (2.5)$$

and β is the swirl ratio:

$$\beta = \frac{V_\phi}{\Omega b} \quad (2.6)$$

The mass flow rates for egress and ingress can be obtained by integrating the velocities across the seal clearance. These equations are applicable to both RI and EI ingress. It can be seen from eqs (2.3) and (2.4) that swirl in the wheel-space increases egress, which is often referred to as the *disc-pumping effect*; conversely, swirl in the annulus decreases ingress. It should also be noted that egress can occur even if $p_2 > p_1$, which is always the case for RI ingress.

2.3 Nondimensional sealing parameter

The nondimensional sealing parameter, Φ_o , combines the effects of $C_{w,o}$, G_c and Re_ϕ into a single variable:

$$\Phi_o = \frac{C_{w,o}}{2\pi G_c Re_\phi} \quad (2.7)$$

As Re_ϕ and $C_{w,o}$ include viscous terms which cancel in the above equation, this definition disguises the fact that Φ_o is an inertial parameter. It is more appropriate to use an alternative definition, which is equivalent to eq (2.7):

$$\Phi_o = \frac{U}{\Omega b} \quad (2.8)$$

where U is the bulk mean radial velocity of sealing air through the seal clearance, so that

$$U = \frac{\dot{m}_o}{2\pi \rho b s_c} \quad (2.9)$$

The symbols Φ_e , Φ_i and Φ_o denote the parameters for egress, ingress and the sealing flow, respectively. Φ_{min} is the value of Φ_o when the system is sealed, so that

$$\Phi_{min} = \frac{U_{min}}{\Omega b} = \frac{C_{w,min}}{2\pi G_c Re_\phi} \quad (2.10)$$

From the continuity equation,

$$\Phi_o = \Phi_e - \Phi_i \quad (2.11)$$

and, for $\Phi_o < \Phi_{min}$, the sealing effectiveness can be calculated from

$$\varepsilon = 1 - \frac{\Phi_i}{\Phi_e} = \frac{\Phi_o}{\Phi_e} = \frac{\Phi_o}{\Phi_o + \Phi_i} \quad (2.12)$$

That is, $\varepsilon = 0$ when $\Phi_o = 0$, and $\varepsilon = 1$ when $\Phi_o = \Phi_{min}$.

Although the effectiveness is a convenient parameter, the designer wants to know how much hot gas enters the wheel-space when $\Phi_o < \Phi_{min}$. This involves calculating Φ_i where from eq (2.12)

$$\frac{\Phi_i}{\Phi_o} = \varepsilon^{-1} - 1 \quad (2.13)$$

Another parameter that is widely used in the orifice equations is Γ_c , the ratio of the discharge coefficients, which is defined by

$$\Gamma_c = \frac{C_{d,i}}{C_{d,e}} \quad (2.14)$$

For RI ingress - where the external flow is axisymmetric and where there is no circumferential variation of external pressure - C_{β_1} , the internal swirl parameter, is the driving force for ingress.

The model provides a simple equation that expresses ε , the sealing effectiveness, in terms of Φ_o , and the correlation between this equation and a measured value of ε and Φ_o depends on only two empirical parameters. Furthermore, the model has the important advantage of providing an estimate of $\Phi_{min,RI}$ from the (ε , Φ_o) data points without requiring any details of the distribution of pressure or swirl in the wheel-space.

2.4 Solutions of orifice equations for RI ingress

From eq (A1) of Appendix A,

$$\Phi_{min,RI} = C_{d,e} C_{\beta_1}^{1/2} \quad (2.15)$$

where C_{β_1} is the swirl parameter defined by eq (2.5). The effectiveness equations for $\Phi_o < \Phi_{min,RI}$ are given in Appendix A as

$$\frac{\Phi_o}{\Phi_{min,RI}} = \frac{\varepsilon}{[1 + (1 - \varepsilon)^{1/2}][1 + \Gamma_c^{-2}(1 - \varepsilon)]^{1/2}} \quad (2.16)$$

For $\Phi_o > \Phi_{min,RI}$, $\varepsilon = 1$.

The ingress parameter, $\Phi_{i,RI}$, can be found from eqs (2.13) and (2.16), so that

$$\frac{\Phi_{i,RI}}{\Phi_{min,RI}} = \frac{1 - \varepsilon}{[1 + (1 - \varepsilon)^{1/2}][1 + \Gamma_c^{-2}(1 - \varepsilon)]^{1/2}} \quad (2.17)$$

In the limit that $\Phi_o = 0$, where $\varepsilon = 0$, eq (2.17) reduces to

$$\frac{\Phi_{i,RI}^*}{\Phi_{min,RI}} = \frac{1}{2[1 + \Gamma_c^{-2}]^{1/2}} \quad (2.18)$$

$\Phi_{i,RI}^*$ denotes the value of $\Phi_{i,RI}$ when $\Phi_o = 0$, and this is the maximum value of the nondimensional ingested flow rate that can enter the wheel-space. For $\Gamma_c = 1$, $\Phi_{i,RI}^* / \Phi_{min,RI} = 0.35$; that is, for this case the maximum flow that can be ingested is 35% of the flow required to seal the system.

It should be noted that the empirical constants, $C_{d,i}$ and $C_{d,e}$, which appear in the orifice equations, have been replaced by the unknown parameters, $\Phi_{min,RI}$ and Γ_c , which appear in the effectiveness equations. Values of these two parameters can be estimated using statistical fitting techniques, as described below. It should also be noted that the effectiveness equations require no knowledge of the value of C_{β_1} , the internal swirl parameter.

Zhou *et al.* [16] used the method of maximum likelihood estimation to fit the theoretical curves produced from the effectiveness equations to the RI ingress data obtained by Graber *et al.* [15]. The theoretical curves were shown to be in good agreement with the experimental data, which were obtained for a variety of seals for a number of different external swirl ratios and rotational Reynolds numbers. This statistical method provides the best estimates of the two unknown parameters, $\Phi_{min,RI}$ and Γ_c , and it also provides the confidence intervals in these estimates.

3. MEASUREMENTS OF RIM-SEAL EFFECTIVENESS

3.1 Experimental method

The new research facility which experimentally simulates hot gas ingestion into the wheel space of an axial turbine stage using CO₂ tracer gas, was described in Part 1. The test section of the facility, shown in Fig. 3, featured a turbine stage with 32 vanes and 41 blades.

For the RI ingestion tests presented here, the inlet to the annulus was closed but the outlet was open to the atmosphere. As the stationary vanes and rotating blades were still present in the annulus, rotation of the disc would have created swirl in the external fluid. However, as found by Graber *et al.* [15], the external swirl did not appear to affect RI ingress. (This is shown below where the measured value of $\Phi_{min,RI}$ for the axial-clearance seal is unaffected by rotational speed and its value is close to that of Bayley and Owen for RI ingress.)

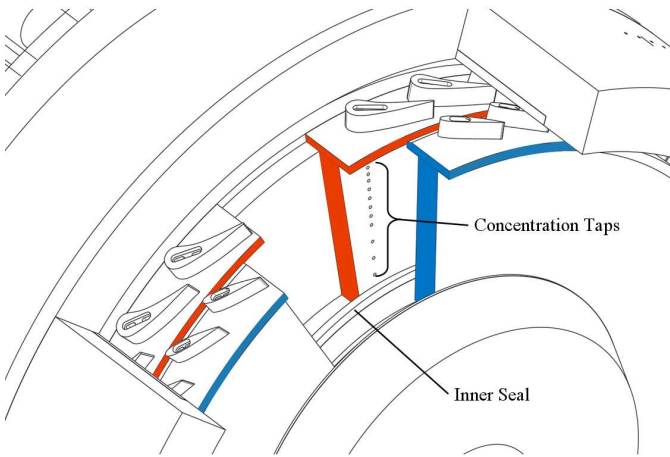


Fig. 3: Experimental test section

The disc could be rotated up to speeds of 4000 rpm, providing a maximum rotational Reynolds numbers, Re_ϕ (based on disc radius) up to 1.1×10^6 . Rotating fluid in the wheel-space created a radial gradient of pressure, so that the pressure inside the cavity was sub-atmospheric. The pumping action of the rotating disc caused a radial outflow of fluid, or egress, in the disc boundary layer, and the low pressure in the wheel-space caused ingress of external fluid through the rim seal into the cavity.

Sealing air was introduced into the wheel-space at a low radius through an inner seal. Increasing this superposed radial flow rate increased the relative pressure inside the wheel-space and consequently reduced the amount of ingested air. At sufficiently high superposed flow rates ingress did not occur.

To measure the degree of ingestion, this sealing flow was seeded with a carbon dioxide tracer gas. The variation of CO₂ gas concentration with radius ($0.55 < r/b < 0.993$) along the stator in the wheel-space was determined by sampling at 15 radial locations as illustrated in Fig. 3. As in Part 1, these measurements were used to determine the variation of ε_c (the

effectiveness based on concentration on the stator at $r/b = 0.958$) with sealing flow rate. The effectiveness data is presented in terms of $C_{w,o}$, the non-dimensional sealing flow rate, as well as Φ_θ , the sealing parameter. The experimental data is compared with theoretical calculations from the orifice model using the effectiveness equations, eqs (2.16) and (2.17), and the fitting method of Zhou *et al.* [16].

The two rim seals investigated in the RI ingress experiments are the same as those described and used in Part 1. The stationary values of G_c were 0.0105 and 0.126 for the axial- and radial-clearance seals respectively; for the radial-clearance seal, G_c decreased to 0.119 at $Re_\phi \sim 10^6$.

It should be noted that the effectiveness measured by concentration was calculated from

$$\varepsilon_c = \frac{c_s - c_a}{c_o - c_a} \quad (3.1)$$

where the subscripts a, o and s refer respectively to the air in the annulus, the sealing air at inlet to the system and the stator surface. From eq (2.13) for the ingress parameter, it follows that

$$\frac{\Phi_{i,RI}}{\Phi_o} = \frac{c_o - c_s}{c_s - c_a} \quad (3.2)$$

3.2 Radial variation of effectiveness on stator surface

The flow structure in a rotating-disc system depends on the value of λ_T , the turbulent flow parameter [17]. A value of $\lambda_T = 0.22$ is associated with the flow rate entrained by a free disc, and – depending on the radius ratio of the wheel-space - values above this level are expected to suppress the core rotation in the wheel-space.

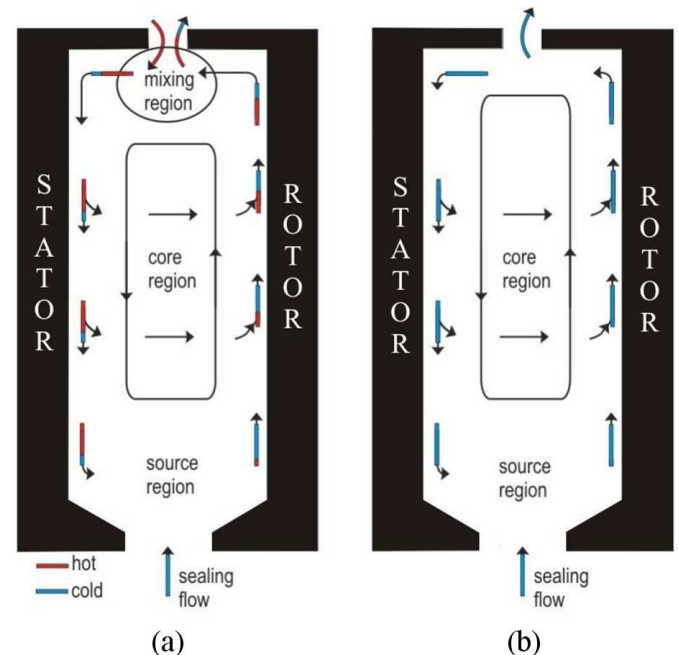


Fig. 4: Simplified diagram of ingress and egress
(a) $\Phi_\theta < \Phi_{min}$ (b) $\Phi_\theta = \Phi_{min}$

In the experiments conducted here, where $\lambda_T \ll 0.22$, the flow structure is expected to be similar to that shown in Fig. 4, which was based on the computational fluid dynamics described in [18]. There are separate boundary layers on the rotating and stationary discs with a rotating core of inviscid fluid between the layers. Radial inflow occurs inside the boundary layer on the stator and outflow occurs inside that on the rotor; fluid migrates axially across the core from the stator to the rotor.

As discussed in [17, 19-20], the flow in an inviscid rotating fluid is governed by Coriolis forces. For small relative velocities, where the Taylor-Proudman theorem applies, all components of velocity are independent of z , the axis of rotation. For rotating flow over a stationary disc, the fluid flows radially *inward* in the boundary layer and there is an axial flow *away from* the disc into the rotating core; for rotating flow over a rotating disc - where $V_\phi < \Omega r$ - the fluid flows radially *outward* and there is an axial flow from the core *towards* the disc.

Ingress affects this flow structure. The ingested fluid mixes with the sealing flow in a small mixing region near the rim seal. The mixed fluid then flows radially inward in the stator boundary layer, from where it is progressively entrained into the boundary layer on the rotor. If the flow is completely mixed in the outer mixing region then the concentration on the stator wall will be invariant with radius. (For an adiabatic stator with negligible frictional heating, the wall temperature would also be invariant with radius.)

The core region is diminished in size and pushed to slightly higher radius (see Fig. 4b), as the wheel-space is pressurised and the superimposed sealing flow rate increased to $\Phi_{min,RI}$.

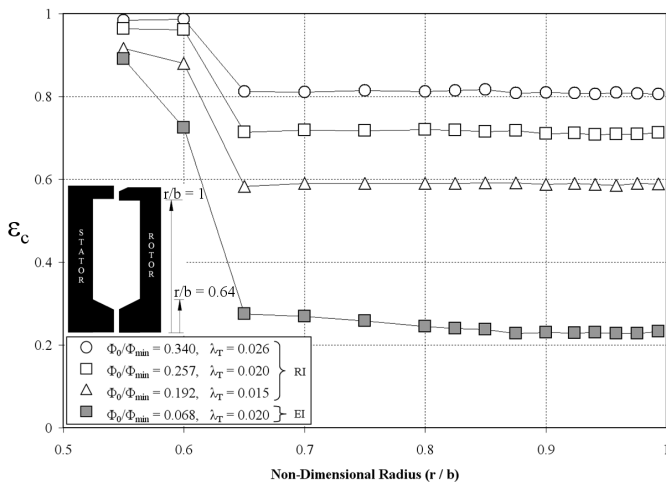


Fig. 5: Effect of sealing flow rate on measured radial variation of effectiveness on stator surface for axial-clearance seal. Open symbols denote RI ingress; solid symbols denote EI ingress.

Figure 5 shows the radial variation of ϵ_c on the stator surface for tests at $Re_\phi = 5.3 \times 10^5$ for the axial-clearance seal; results

for a test with EI ingress are shown for comparison. The tests were conducted for several values of Φ_0/Φ_{min} and λ_T ; in all cases ingress occurred.

As expected, ϵ_c increases as Φ_0/Φ_{min} increases. For the RI tests, the effectiveness is virtually invariant with radius for $r/b > 0.65$, which suggests that complete mixing has occurred in a region very close to the rim seal. (The rapid increase in ϵ_c at the smaller radii is caused by the presence of the inner seal, which prevents, or strongly reduces, the ingestion of fluid into the 'inner wheel-space' where the sealing flow is introduced.)

Figure 5 also shows effectiveness data for an EI test, also at $Re_\phi = 5.3 \times 10^5$ (conducted as part of the test programme described in Part 1). For $r/b > 0.65$, the small increase of ϵ_c with decreasing radius suggests that incomplete mixing occurred in the region near the rim seal. The consequential concentration gradient in the stator boundary layer means that the value of ϵ_c on the stator surface is slightly smaller than that in the core.

EI ingress is discussed in detail in Part 1 but it is useful to compare the effectiveness distributions for EI with those for RI ingress. This comparison can be seen in Fig. 5 for $\lambda_T = 0.020$, which corresponds to the same value of Φ_0 for both cases. The sealing effectiveness for the RI case is significantly greater than that for the EI case: for the same sealing flow rates, EI ingress causes much more ingestion.

For the results presented below, the effectiveness values were based on the concentration measurements on the stator surface at $r/b = 0.958$.

3.3 Variation of effectiveness with sealing flow rate

Fig. 6 shows the effect of Re_ϕ on the variation of effectiveness with $C_{w,o}$, the nondimensional sealing flow rate, for the two rim seals with RI ingress. A thumb-nail sketch of the seal geometries is shown on this and all following figures.

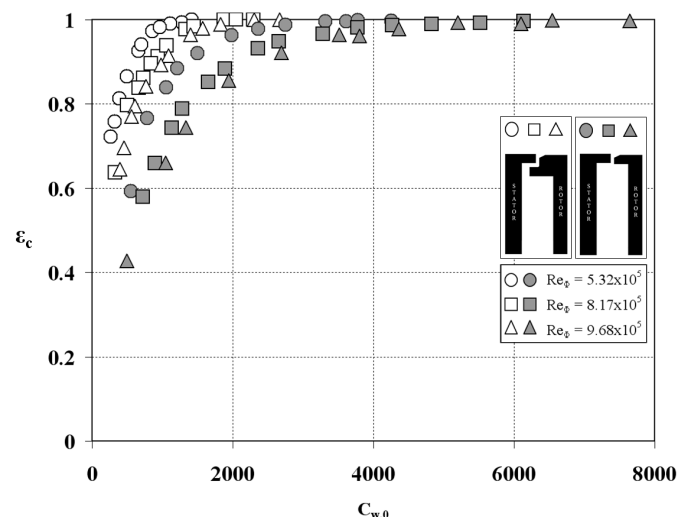


Fig. 6: Effect of Re_ϕ on measured variation of ϵ_c with $C_{w,o}$ for RI ingress. (Open symbols denote radial-clearance seal; solid symbols denote axial-clearance seal.)

The figure illustrates that ε_c increases with increasing $C_{w,o}$, as the sealing flow pressurises the wheel-space and reduces ingestion through the rim-seal. Even allowing for the small difference between the values of G_c for the two seals, the radial-clearance seal is the more effective one. For both seals, ε_c decreases as Re_ϕ increases.

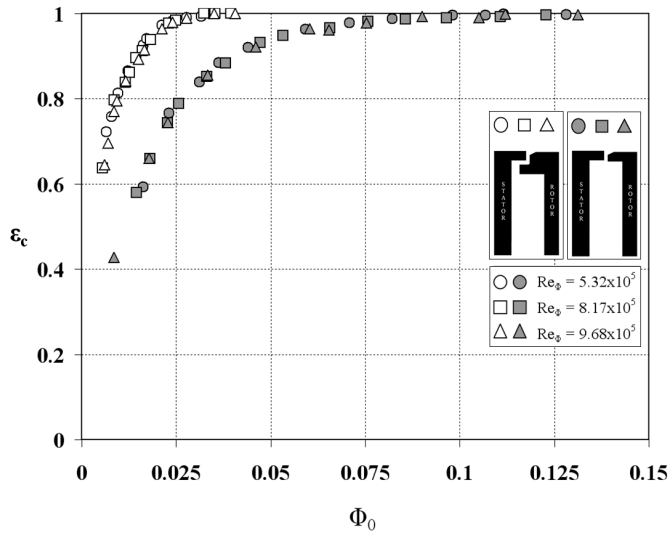


Fig. 7: Measured variation of sealing effectiveness with Φ_0 for RI ingress. (Open symbols denote radial-clearance seal; solid symbols denote axial-clearance seal.)

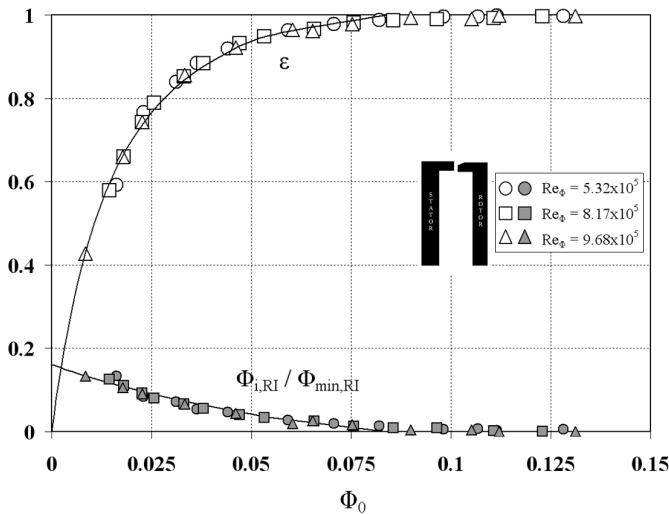


Fig. 8: Comparison between theoretical effectiveness curves and experimental data for axial-clearance seal with RI ingress. (Open symbols denote ε data; closed symbols denote $\Phi_{i,RI}/\Phi_{min,RI}$ data; solid lines are theoretical curves.)

In Fig. 7, the data shown in Fig. 6 have been re-plotted versus Φ_0 . Instead of having to use separate correlations for

the effects of G_c and Re_ϕ on ε , Φ_0 combines $C_{w,o}$, G_c and Re_ϕ into a single flow parameter and collapses all the data. (As stated above, the radial-clearance seal has slightly varying values of G_c at different Re_ϕ .)

Figs 8 and 9 show comparisons between the theoretical effectiveness curves and the experimental data for the two seals. The curves were based on eqs (2.16) and (2.17), which were fitted to the data using the method of Zhou *et al.* [16].

The estimated values of $\Phi_{min,RI}$ and Γ_c and their 95% confidence intervals are shown in Table 1 together with the values for EI ingress from Part 1. The values of n , the number of data points used in the fits, and σ , the standard deviation between the data and the fitted curves, are also shown in the table. (Zhou *et al.* suggest that there should be at least 16 data points for an accurate estimate of $\Phi_{min,RI}$, a condition that is satisfied here.)

From the Bayley-Owen criterion for an axial-clearance seal, $\Phi_{min,RI} = 0.097$; this is around 13% larger than the value shown in Table 1. However, Bayley and Owen used pressure and not concentration measurements to determine their correlation. It can also be seen from Table 1 that the confidence intervals are around 10% of the estimated value of $\Phi_{min,RI}$. As Fig. 8 shows, is very difficult to determine the precise value of Φ_0 when ε first equals unity, and there is a consequential uncertainty in the determination of $\Phi_{min,RI}$. (The value of Φ_0 at $\varepsilon = 0.95$ has a smaller uncertainty, and there is a case for using this rather than Φ_{min} as a design criterion for RI and EI ingress.)

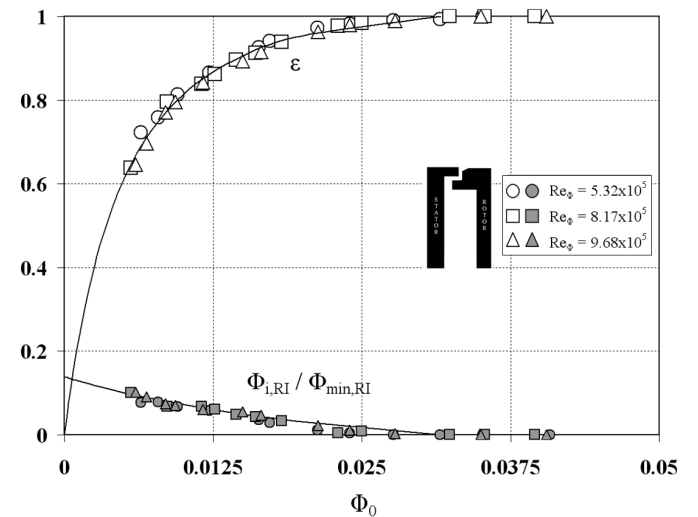


Fig. 9: Comparison between theoretical effectiveness curves and experimental data for radial-clearance seal with RI ingress. (Open symbols denote ε data; closed symbols denote $\Phi_{i,RI}/\Phi_{min,RI}$ data; solid lines are theoretical curves.)

Both figures show very good agreement between the theoretical curves and the data; the good agreement is confirmed by the relatively small values of σ in Table 1. The estimated values of $\Phi_{min,RI}$ are 0.0838 and 0.0317 for the axial-

clearance and radial-clearance seals respectively. This shows that, to prevent ingestion for RI ingress, the radial-clearance seal requires approximately 38% of the air required for the axial-clearance seal.

Figs 8 and 9 also show the variation of $\Phi_{i,RI} / \Phi_{min,RI}$ with Φ_0 according to eq (2.17). This variation is of importance to the seal designer as it shows how much ingested flow enters the wheel-space when $\varepsilon < 1$. Table 1 includes values of $\Phi_{i,RI}^*$; this is the maximum value of $\Phi_{i,RI}$, which occurs when $\Phi_0 = 0$. It follows from the values in the table that $\Phi_{i,RI}^* / \Phi_{min,RI} = 0.17$ for the axial-clearance seal and 0.14 for the radial-clearance seal. That is, for either seal, the maximum ingress is only a relatively small fraction of the flow rate needed to prevent ingestion.

Seal	RI ingress		EI ingress	
	Axial clearance	Radial clearance	Axial clearance	Radial clearance
$\hat{\Phi}_{min}$	0.0838	0.0317	0.326	0.0915
$\hat{\Phi}_{min}^-$	0.0773	0.0296	0.309	0.0869
$\hat{\Phi}_{min}^+$	0.0921	0.0342	0.344	0.0962
Φ_i^*	0.0135	0.00446	0.0764	0.0371
$\hat{\Gamma}_c$	0.342	0.288	0.476	1.32
$\hat{\Gamma}_c^-$	0.297	0.257	0.421	1.09
$\hat{\Gamma}_c^+$	0.390	0.320	0.545	1.63
n	38	36	60	54
σ	0.0121	0.00986	0.0146	0.0184

Table 1: Parameters for axial-clearance and radial-clearance seals for RI and EI ingress. (^ denotes estimated value from the theoretical curve, and + - denote upper and lower bounds of 95% confidence intervals.)

3.4 Comparison of seal performance for EI and RI ingress

Fig. 10 shows the effectiveness data and theoretical curves for both seals with EI and RI ingress; the EI results were also presented in Part 1. It can be seen from Table 1 that, for RI ingress, the ratio of Φ_{min} for the radial-clearance seal to that required for the axial-clearance seal is around 38%; for EI ingress, the ratio is around 26%. That is, for both EI and RI ingress, the radial-clearance seal is significantly more effective than the axial-clearance seal. This result is consistent with the experiments of Phadke and Owen [11] for RI ingress and Bohn and Wolff [21] for EI ingress. It can also be seen from Table 1 that the value of Φ_{min} for an axial-clearance seal for RI ingress is similar to that for a radial-clearance seal for EI ingress.

In [2], it was suggested that EI ingress only occurs when $\Phi_{min} > 2 \Phi_{min,RI}$ and combined ingress occurs below this limit. In the experiments conducted here, the ratio of EI to RI ingress was 3.9 and 2.9 for the axial- and radial-clearance seals

respectively. These values confirm that the EI tests should be outside the combined-ingress region.

4. PRACTICAL IMPLICATIONS

The results presented in both parts of this paper address important design questions: how much sealing air is required to prevent ingestion and when ingress occurs how much gas enters the wheel-space? The experiments, the orifice model and the statistical technique used to fit the theoretical curves to the data provide a powerful way of quantifying the answers to both these questions. The combined techniques of experiment, theory and statistics are valuable tools, which used carefully should be of value to the designer.

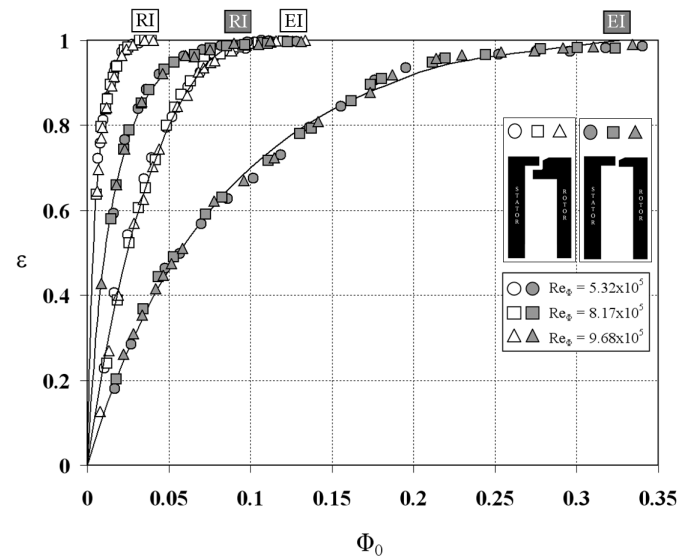


Fig. 10: Comparison of sealing effectiveness for EI and RI ingress. (Open symbols denote radial-clearance seal; solid symbols denote axial-clearance seal; solid lines are theoretical curves.)

There are, however, some important questions that remain to be addressed. What is the effect of ingested hot gas on the heat transfer to the metal surfaces in the turbine wheel-space? Can the results obtained from an experimental rig operating at incompressible-flow conditions (which was the case for most of the experiments described here) be extrapolated to engine conditions? What happens to the sealing effectiveness at off-design conditions? Can the methods used here for simple single rim seals be used to optimise complex double seals? Research at the University of Bath is directed at answering these important questions, and the results will be the subject of future publications.

Work is also underway to investigate the effect of ingested hot gas on the heat transfer to the surfaces inside the wheel-space. Measurements of the temperature of the fluid in the wheel-space, using fast response thermocouples, and the surface temperature of the rotor and stator, using thermochromic liquid

crystal (TLC) will be taken. Together with the reported concentration measurements, these temperatures should enable the determination of not only the adiabatic sealing effectiveness but also the Nusselt numbers for both the rotor and the stator surfaces. As discussed in [18], computational fluid dynamics will have its part to play in this research.

5. CONCLUSIONS

The experimental rig described in Part 1 of this two-part paper was used to determine the sealing effectiveness, ε_c , which was based on concentration measurements using CO₂ as the tracer gas. Two different seals were tested, and rotationally-induced (RI) ingress was achieved by running the rig at different rotational speeds with no axial flow through the external annulus. The theoretical curves obtained from an orifice model were fitted to the experimental data using the statistical method of maximum likelihood estimates.

The principal conclusions are as follows:

- Using, Φ_0 , the nondimensional sealing parameter, the effectiveness data obtained at different rotational speeds could be collapsed onto a single curve; this was also the case for EI ingress in Part 1.
- There was very good agreement between the experimental measurements and the theoretical effectiveness curves (and with the theoretical ingress curves) obtained from the RI orifice model.
- For RI ingress, the ratio of the sealing flow rate required to prevent ingress for the radial-clearance seal to that required for the axial-clearance seal was around 38%.
- For the axial-clearance seal, the ratio of the sealing flow rate required to prevent ingress for the RI case to that required for the EI case was around 26%; for the radial-clearance seal, the ratio was around 35%.

ACKNOWLEDGEMENTS

The authors also wish to thank the China Scholarship Council and Beihang University, Beijing, China, for supporting Kunyuan Zhou during his stay at the University of Bath. The research described here is part of a programme jointly funded by the UK Engineering and Physical Sciences Research Council, Siemens Fossil Power Generation and Siemens Oil & Gas.

REFERENCES

[1] Sangan, C. M., Pountney, O. J., Zhou, K., Wilson, M., Owen, J. M., and Lock, G. D., 2011, "Experimental Measurements of Ingestion through Turbine Rim Seals. Part 1: Externally-Induced Ingress," ASME Paper GT2011-45310.

[2] Owen, J. M., Pountney, O. J., and Lock, G. D., 2010, "Prediction of Ingress Through Turbine Rim Seals. Part 2: Combined Ingress," ASME Paper GT2010-23349. To appear in ASME J.Turbomach.

[3] Owen, J.M., 2011, "Prediction of Ingestion Through Turbine Rim Seals---Part I: Rotationally Induced Ingress"; ASME J. Turbomach., Vol. 133, Issue 3, 031005-1 to 9.

[4] Owen, J.M., 2011, "Prediction of Ingestion Through Turbine Rim Seals---Part II: Externally Induced and Combined Ingress"; ASME J. Turbomach., Vol. 133, Issue 3, 031006-1 to 9.

[5] Owen, J. M., Pountney, O. J., Zhou, K., Wilson, M., and Lock, G. D., 2010, "Prediction of Ingress Through Turbine Rim Seals. Part 1: Externally-Induced Ingress," ASME Paper GT2010-23346. To appear in ASME J.Turbomach.

[6] Bayley, F. J., and Owen, J. M., 1970, "Fluid Dynamics of a Shrouded Disk System with a Radial Outflow of Coolant," Journal of Engineering for Power, 92, pp. 335-341.

[7] Chew, J. W., 1991, "A Theoretical Study of Ingress for Shrouded Rotating Disk Systems With Radial Outflow," ASME J.Turbomach., 113(1), pp. 91-97.

[8] Chew, J. W., Dadkhah, S., and Turner, A. B., 1992, "Rim Sealing of Rotor--Stator Wheelspaces in the Absence of External Flow," ASME J.Turbomach., 114(2), pp. 433-438.

[9] Dadkhah, S., Turner, A. B., and Chew, J. W., 1992, "Performance of Radial Clearance Rim Seals in Upstream and Downstream Rotor--Stator Wheelspaces," ASME J.Turbomach., 114(2), pp. 439-445.

[10] Phadke, U. P., and Owen, J. M., 1983, "An Investigation Of Ingress For An Air-Cooled Shrouded Rotating-Disk System With Radial-Clearance Seals," J. Eng. Power-Trans. ASME, 105(1), pp. 178-183.

[11] Phadke, U. P., and Owen, J. M., 1988, "Aerodynamic Aspects of the Sealing of Gas-Turbine Rotor-Stator Systems : Part 1: The Behavior of Simple Shrouded Rotating-Disk Systems in a Quiescent Environment," Int. J. Heat Fluid Flow, 9(2), pp. 98-105.

[12] Phadke, U. P., and Owen, J. M., 1988, "Aerodynamic Aspects of the Sealing of Gas-Turbine Rotor-Stator Systems : Part 2: The Performance of Simple Seals in a Quasi-Axisymmetric External Flow," Int. J. Heat Fluid Flow, 9(2), pp. 106-112.

[13] Phadke, U. P., and Owen, J. M., 1988, "Aerodynamic Aspects of the Sealing of Gas-Turbine Rotor-Stator Systems : Part 3: The Effect of Nonaxisymmetric External Flow on Seal Performance," Int. J. Heat Fluid Flow, 9(2), pp. 113-117.

[14] Daniels, W. A., Johnson, B. V., Graber, D. J., and Martin, R. J., 1992, "Rim Seal Experiments and Analysis for Turbine Applications," ASME J.Turbomach., 114(2), pp. 426-432.

[15] Graber, D. J., Daniels, W. A., and Johnson, B. V., 1987, "Disk Pumping Test, Final Report," Air Force Wright Aeronautical Laboratories, Report No. AWFAL-TR-87-2050.

[16] Zhou, K., Wood, S. N., and Owen, J. M., 2011, "Statistical and Theoretical Models of Ingestion through Turbine Rim Seals," ASME Paper GT2011-45139.

[17] Owen, J. M., and Rogers, R. H., 1989, "Flow and Heat Transfer in Rotating-Disc Systems, Volume 1 - Rotor Stator Systems." Research Studies Press, UK; John Wiley N.Y.

[18] Zhou, K., Wilson, M., Lock, G. D., and Owen, J. M., 2011, "Computation of Ingestion through Gas Turbine Rim Seals," ASME Paper GT2011-45314.

[19] Childs, P. R. N., 2010, "Rotating Flow," Butterworth-Heinemann, Oxford.

[20] Owen, J. M., and Rogers, R. H., 1995, "Flow and Heat Transfer in Rotating-Disc Systems, Volume 2 - Rotating Cavities." Research Studies Press, UK; John Wiley N.Y.

[21] Bohn, D., and Wolff, M., 2003, "Improved Formulation to Determine Minimum Sealing Flow: C_w, \min - for Different Sealing Configurations," ASME Paper GT2003-38465

APPENDIX A: EFFECTIVENESS EQUATIONS FOR RI INGRESS

A1: Derivation of effectiveness equation

The effectiveness equation for RI ingress can be derived from the analysis in [3] and the symbols are defined in the Nomenclature. From Appendix B of [3] the following equations apply for the case of RI ingress where the external swirl is negligible:

$$\Phi_{min,RI} = C_{d,e} C_{\beta_1}^{1/2} \quad (A1)$$

$$\frac{\Phi_e}{\Phi_{min,RI}} = \frac{1 - \Gamma_p}{\Gamma_T} \quad (A2)$$

$$\frac{\Phi_i}{\Phi_{min,RI}} = \frac{\Gamma_c^2 \Gamma_p}{\Gamma_T} \quad (A3)$$

and

$$\frac{\Phi_o}{\Phi_{min,RI}} = \frac{\Phi_e - \Phi_i}{\Phi_{min,RI}} = \frac{1 - \Gamma_p (1 + \Gamma_c^2)}{\Gamma_T} \quad (A4)$$

where

$$\Gamma_T = [(1 - \Gamma_p)^{1/2} + \Gamma_c \Gamma_p^{1/2}] \quad (A5)$$

Using the above equations, it follows that

$$\varepsilon = 1 - \frac{\Phi_i}{\Phi_e} = \frac{1 - \Gamma_p (1 + \Gamma_c^2)}{1 - \Gamma_p} \quad (A6)$$

Eq (A6) can be rearranged to give

$$\Gamma_p = \frac{1 - \varepsilon}{(1 - \varepsilon) + \Gamma_c^2} \quad (A7)$$

Using eq (A7) to eliminate Γ_p from eq (A4), it follows that for

$$\Phi_o \leq \Phi_{min,RI} \quad (A8)$$

$$\frac{\Phi_o}{\Phi_{min,RI}} = \frac{\varepsilon}{[1 + (1 - \varepsilon)^{1/2}][1 + \Gamma_c^{-2} (1 - \varepsilon)]^{1/2}}$$

For $\Phi_o > \Phi_{min,RI}$, $\varepsilon = 1$.

Eq (A8) is referred to as the *RI effectiveness equation*.

A2: Ingested flow rate for RI ingress

The sealing effectiveness is a useful parameter, which is usually determined from concentration measurements in an experimental rig. However, it is also useful for the designer to

be able to estimate Φ_i , the nondimensional flow rate of air that enters the wheel-space when $\Phi_o < \Phi_{min}$.

From eq (A1)

$$\varepsilon = \frac{\Phi_o}{\Phi_{e,RI}} = \frac{\Phi_o}{\Phi_o + \Phi_{i,RI}} \quad (A9)$$

and so

$$\frac{\Phi_{i,RI}}{\Phi_o} = \varepsilon^{-1} - 1 \quad (A10)$$

As

$$\frac{\Phi_{i,RI}}{\Phi_{min,RI}} = \frac{\Phi_{i,RI}}{\Phi_o} \frac{\Phi_o}{\Phi_{min,RI}} \quad (A11)$$

it follows from eqs (A8) and (A10) that

$$\Phi_{i,RI} = \Phi_{min,RI} \frac{1 - \varepsilon}{[1 + (1 - \varepsilon)^{1/2}][1 + \Gamma_c^{-2} (1 - \varepsilon)]^{1/2}} \quad (A12)$$

In the limit $\Phi_o = 0$, where $\varepsilon = 0$, eq (A12) reduces to

$$\Phi_{i,RI}^* = \Phi_{min,RI} \frac{1}{2[1 + \Gamma_c^{-2}]^{1/2}} \quad (A13)$$

where * signifies that $\Phi_o = 0$. Eq (A13) gives the value of the maximum flow rate that can be ingested into the wheel-space.

APPENDIX B: EFFECTIVENESS EQUATIONS FOR EI INGRESS

B1: Derivation of effectiveness equation

The effective equation for EI ingress can be derived from the analysis in [4] for the saw-tooth model, and symbols are defined in the Nomenclature.

From Section (3.3) of [4]

$$\Phi_{min,EI} = 2/3 C_{d,e} \Delta C_p^{1/2} \quad (B1)$$

$$\frac{\Phi_o}{\Phi_{min,EI}} = g^{3/2} - \Gamma_c (1 - g)^{3/2}$$

and

$$\varepsilon = 1 - \Gamma_c \left[\frac{1 - g}{g} \right]^{3/2} \quad (B2)$$

By eliminating g , a normalised pressure difference, from eqs (B1) and (B2), it can be shown that for $\Phi_o \leq \Phi_{min,EI}$

$$\frac{\Phi_o}{\Phi_{min,EI}} = \frac{\varepsilon}{[1 + \Gamma_c^{-2/3} (1 - \varepsilon)^{2/3}]^{3/2}} \quad (B3)$$

For $\Phi_o > \Phi_{min,EI}$, $\varepsilon = 1$.

Eq (B3) is referred to as the *EI effectiveness equation*.

B2: Ingested flow rate for EI ingress

As

$$\varepsilon = \frac{\Phi_o}{\Phi_{e,EI}} = \frac{\Phi_o}{\Phi_o + \Phi_{i,EI}} \quad (B4)$$

It follows that

$$\frac{\Phi_{i,EI}}{\Phi_o} = \varepsilon^{-1} - 1 \quad (\text{B5})$$

Also, as

$$\frac{\Phi_{i,EI}}{\Phi_{min,EI}} = \frac{\Phi_{i,EI}}{\Phi_o} \frac{\Phi_o}{\Phi_{min,EI}} \quad (\text{B6})$$

it follows from eqs (B3) and (B5) that

$$\Phi_{i,EI} = \Phi_{min,EI} \frac{1 - \varepsilon}{[1 + \Gamma_c^{-2/3} (1 - \varepsilon)^{2/3}]^{3/2}} \quad (\text{B7})$$

In the limit $\Phi_o = 0$, where $\varepsilon = 0$, eq (B7) reduces to

$$\Phi_{i,EI}^* = \Phi_{min,EI} \frac{1}{[1 + \Gamma_c^{-2/3}]^{3/2}} \quad (\text{B8})$$

where * signifies that $\Phi_o = 0$. Eq (B8) gives the value of the maximum flow rate that can be ingested into the wheel-space.